Buckling versus Crystal Expulsion Controlled by Deformation Rate of Particle-Coated Air Bubbles in Oil

Saha, Saikat; Pagaud, Francis; Binks, Bernard P.; Garbin, Valeria

DOI
10.1021/acs.langmuir.1c03171

Publication date
2021

Document Version
Final published version

Published in
Langmuir

Citation (APA)
Saha, S., Pagaud, F., Binks, B. P., & Garbin, V. (2021). Buckling versus Crystal Expulsion Controlled by Deformation Rate of Particle-Coated Air Bubbles in Oil. *Langmuir*, *38*(3), 1259-1265. https://doi.org/10.1021/acs.langmuir.1c03171

LANGMUIR

pubs.acs.org/Langmuir Article

Buckling versus Crystal Expulsion Controlled by Deformation Rate of Particle-Coated Air Bubbles in Oil

Saikat Saha, Francis Pagaud, Bernard P. Binks, and Valeria Garbin*

Cite This: *Langmuir* 2022, 38, 1259−1265 Read Online

ACCESS | Metrics & More | Article Recommendations | Supporting Information

ABSTRACT: Oil foams stabilized by crystallizing agents exhibit outstanding stability and show promise for applications in consumer products. The stability and mechanics imparted by the interfacial layer of crystals underpin product shelf life, as well as optimal processing conditions and performance in applications. Shelf life is affected by the stability against bubble dissolution over a long time scale, which leads to slow compression of the interfacial layer. In processing flow conditions, the imposed deformation is characterized by much shorter time scales. In practical situations, the crystal layer is therefore subjected to deformation on extremely different time scales. Despite its importance, our understanding of the behavior of such interfacial layers at different time scales remains limited. To address this gap, here we investigate the dynamics of single, crystal-coated bubbles isolated from an oleofoam, at two extreme time scales: the diffusion-limited time scale characteristic of bubble dissolution, $\sim 10^4$ s, and a fast time scale characteristic of processing flow conditions, $\sim 10^{-3}$ s. In our experiments, slow deformation is obtained by bubble dissolution, and fast deformation in controlled conditions with real-time imaging is obtained using ultrasound-induced bubble oscillations. The experiments reveal that the fate of the interfacial layer is dramatically affected by the dynamics of deformation: after complete bubble dissolution, a continuous solid layer remains; after fast, oscillatory deformation of the layer, small crystals are expelled from the layer. This observation shows promise toward developing stimuli-responsive systems, with sensitivity to deformation rate, in addition to the already known thermoresponsiveness and photoresponsiveness of oleofoams.

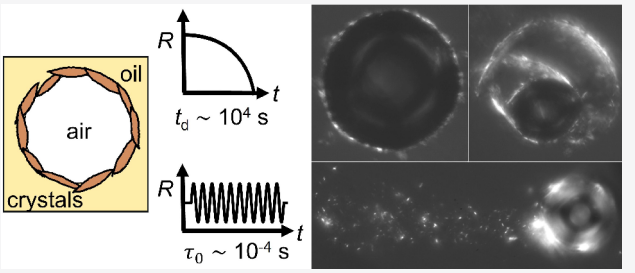

INTRODUCTION

Oil foams have diverse use in pharmaceutical, food, and cosmetic applications.[1,2] While air−oil interfaces are difficult to stabilize with molecular surfactants,[3] various crystallizing agents have been found to confer long-term stability to oil foams[2−8] and novel air-in-oil-in-water systems.[9] Crystals can nucleate and grow both in the bulk oil phase and directly on the oil−air interface, upon decreasing the temperature of a preheated solution.[10] Crystals formed in the bulk can then adsorb to the air−oil interfaces during mixing, while excess crystals can form a network in the oil phase (*i.e.*, an oleogel).[5] In this case, foam stability is due to both the bulk and interfacial networks of crystals.[11,12] Much progress has been made in understanding the formation and stability of oil foams stabilized by crystallizing agents, yet our knowledge of the mechanical properties and dynamic behaviors of such systems remains limited, despite its importance for product shelf life, as well as optimal processing conditions and performance in applications. In particular, while there is significant literature available on the rheology of oleogels formed by the crystal network in the bulk oil phase,[1,2] and on the link between crystal formation and network properties,[13,14] less is understood about the microstructure and properties of the crystal-stabilized interfaces.[15]

The stability, dynamics, and mechanics of particle-stabilized (or "armored") bubbles[16] have been studied extensively for model systems stabilized by micrometer-scale colloids; these studies provided important fundamental insights thanks to the ability to directly visualize the interface microstructure and its evolution. At high surface coverage, particle jamming at the interface supports anisotropic stresses, which oppose the shape-minimizing effects of surface tension and lead to stable, non-spherical bubbles.[16] If the particles have attractive interactions, the sufficient condition to arrest bubble dissolution depends on the surface viscoelasticity[17] rather than surface coverage. Such attractive interactions can be tuned by modifying the particle shape, size, roughness, or surface chemistry.[17] In addition to surface coverage and interparticle interactions, the morphology and deformation of the interfacial monolayer can also depend on the particle-to-bubble size ratio.[18−21] Upon forced dissolution of particle-stabilized

Received: November 26, 2021
Revised: January 4, 2022
Published: January 13, 2022

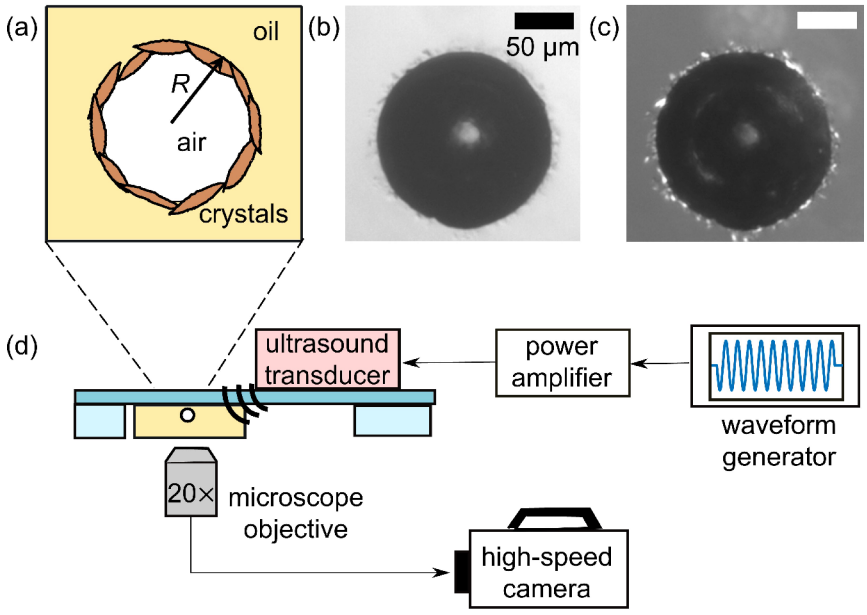

Figure 1. (a) Schematic of an air bubble stabilized by wax crystals in oil. (b) Wax-coated bubble viewed using bright-field microscopy. (c) The same bubble viewed under crossed polarizers. (d) Schematic of the experimental setup.

bubbles, in both aqueous[22] and nonaqueous[23] media, either expulsion of particles or detachment of a continuous layer from the interface was observed, while for ultrafast deformation of colloid-coated bubbles in water forced by ultrasound, buckling of the monolayer and particle expulsion were observed.[24]

In this work, we explore the dynamic response to deformation of wax crystal stabilized bubbles isolated from the bulk crystal network of an oleofoam. We exploit bubble dissolution to apply slow interfacial compression on a diffusion-limited time scale, 10^3–10^4 s, important for product stability and shelf life.[25] Using ultrasound-driven bubble oscillations, we apply compression/expansion on a very fast time scale, 10^{-4} s, relevant in production processes[26] and performance in applications. The experiments reveal a striking difference in the fate of the interfacial wax crystal layer at these two extreme deformation time scales. These insights are also important for optimizing strategies for the design, synthesis, and application of stimuli-responsive systems stabilized by phase-changing materials.[2,27]

MATERIALS AND METHODS

Preparation of Wax Crystal-Coated Bubbles. The wax used (Hydropel QB, Shamrock Technologies) is a blend of paraffin and synthetic waxes with a melting temperature range T_m = 50–105 °C, according to the manufacturer's specifications. The wax particles were used as received. Consumer-grade sunflower oil (Tesco) was used as received. The density was measured to be ρ_{oil} = 0.8879 g cm^{-3} and the viscosity η_{oil} = 50 mPa s at T = 25 °C. The protocol for oleofoam preparation was provided previously.[11] Briefly, a vial containing 2.5 wt/vol % wax particles in sunflower oil was agitated at 3000 rpm for 2 min to form a well-mixed suspension. The suspension was then heated to T = 90 °C to melt the wax and immediately agitated for 2 min to incorporate air to form the oleofoam. During turbulent mixing, the sample cooled to $T \approx$ 45 °C. The vial was then left undisturbed to cool to room temperature. In this process, the excess wax crystals that are not incorporated on the interfaces of bubbles form a gel network in the oil phase (oleogel) which contributes to the stability of such systems.[11]

To prepare samples with wax-coated bubbles without the bulk gel network, the prepared oleofoam was diluted by placing a small sample (≈20 μL) on a microscope glass slide with a spacer of thickness 1.5 mm and adding sunflower oil to obtain isolated bubbles as schematically shown in Figure 1a. High-magnification optical micrographs suggest that the primary crystal size at the oil/air interface is in the range 1–10 μm (see the Supporting Information).

The wax-coated bubbles, when extracted from the oleofoam and re-suspended in sunflower oil, still have their interfacial layers present, as confirmed by their textured interfaces and buckled shapes, visible in Figure 1b, recorded in bright field with an inverted microscope (IX71, Olympus) and digital camera (DCC1645C, Thorlabs). Using crossed polarizers, the layer of crystals is more clearly visible, as shown in Figure 1c. Wherever these crystals can be seen, the interface exhibits non-uniform curvature. Conversely, in regions devoid of crystals, the curvature is uniform. This is characteristic of a cohesive interfacial layer, which does not expand to fill the entire available area.

Bubble Dissolution Experiments. We exploit the phenomenon of bubble dissolution to access long time scales of interface deformation. In the absence of an interfacial layer, the characteristic time scale for bubble dissolution can be estimated[28] by integrating the equation governing the rate of change of radius from the Epstein and Plesset theory[29] to give

$$t_d = \frac{{R_0}^2}{3Dk_H}\left(\frac{R_0\rho_g}{2M_w\sigma} + \frac{1}{R_gT}\right) \sim 10^3\text{–}10^4 \text{ s} \quad (1)$$

This long time scale is achieved by selecting bubbles with an initial radius $R_0 \approx$ 100 μm. For such small bubbles, the Laplace pressure of the gas–liquid interface, $2\sigma/R_0$ with $\sigma \approx$ 30 mN/m for air–oil interfaces,[25] accelerates dissolution; this effect is described by the first term between parentheses in eq 1. The physicochemical properties affecting t_d are the gas diffusivity in the oil, $D \sim 10^{-10}$ m^2/s for vegetable oils,[25] and the solubility of the gas in the oil, measured by Henry's constant k_H, which for N_2 in nonpolar solvents[23] is on the order of $k_H \sim 10^{-5}$ mol Pa^{-1} m^{-3}. The other parameters are the gas density and molar mass, which for nitrogen are ρ_g = 1.2 kg/m^3 and $M_w = 28 \times 10^{-3}$ kg/mol, respectively; the temperature T = 298 K; and the universal gas constant R_g = 8.31 J mol^{-1} K^{-1}.

For wax-coated bubbles, after they are extracted from the bulk oleogel, the interfacial layer alone is not able to arrest bubble dissolution.[11] The stability imparted by the interfacial layer depends on the initial surface coverage and microstructure, and a large variability in dissolution time t_d of these crystal-coated bubbles is

https://doi.org/10.1021/acs.langmuir.1c03171
Langmuir 2022, 38, 1259–1265

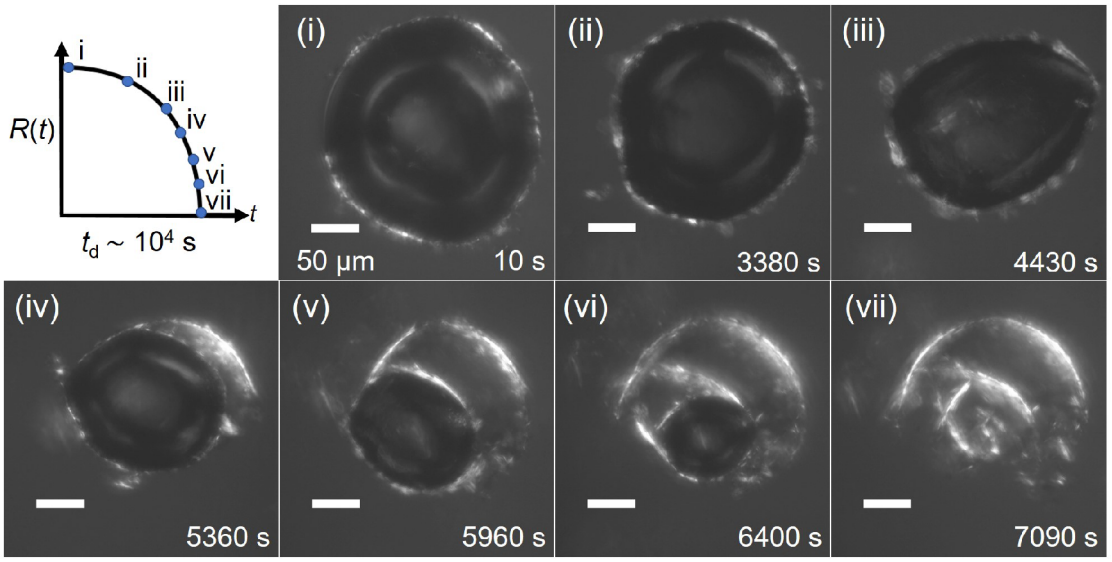

Figure 2. Dissolution of wax crystal-coated bubble in oil (SI Video 1). Schematic of bubble dissolution, occurring over $t \sim 10^3$–10^4 s, with points qualitatively marking the dissolution steps observed in the following panels (i–vii). The image sequence is taken using crossed polarizers.

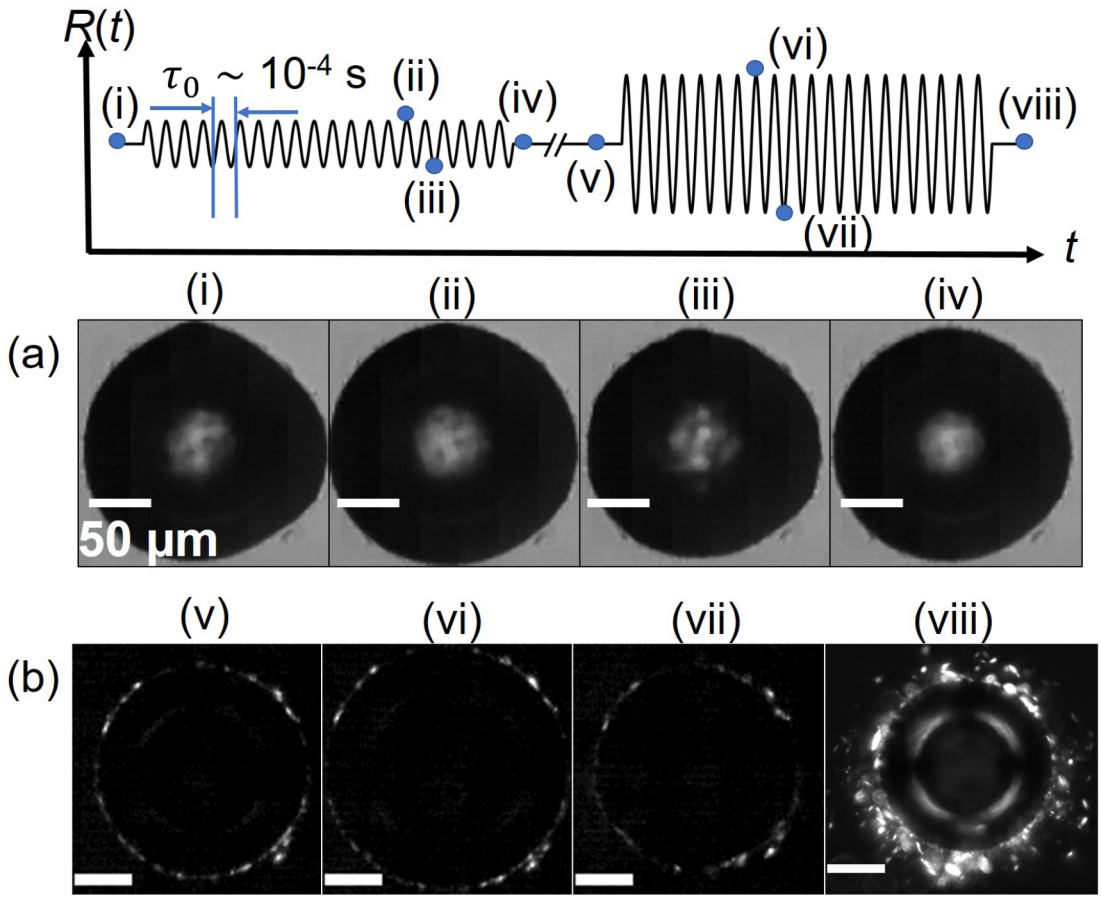

Figure 3. Crystal expulsion after ultrasound-driven bubble oscillations. The schematic illustrates the protocol of oscillating a crystal-coated bubble with ultrasound pulses of different amplitudes. Images at selected times, labeled (i)–(viii), are shown below. (a) High-speed image sequence of a wax-coated bubble with initial radius $R_0 = 101$ μm undergoing oscillations of moderate amplitude, with $x_0 = \Delta R/R_0 \approx 3\%$, $N = 50$ cycles (SI Video 2). The frames show (i) the initial non-spherical shape of the bubble before oscillations, the (ii) maximum and (iii) minimum during oscillations at $f = 25$ kHz, and (iv) the final, almost spherical shape after a total of $N = 260$ cycles of oscillations of small amplitude. (b) High-speed image sequence with crossed polarizers, for large-amplitude oscillations, with $x_0 \approx 20\%$ (SI Video 3): (v) initial state before oscillations, (vi) maximum and (vii) minimum during oscillations at $f = 25$ kHz, and (viii) final state after $N = 100$ cycles of oscillations, showing expulsion of crystals around the bubble.

https://doi.org/10.1021/acs.langmuir.1c03171
Langmuir 2022, 38, 1259–1265

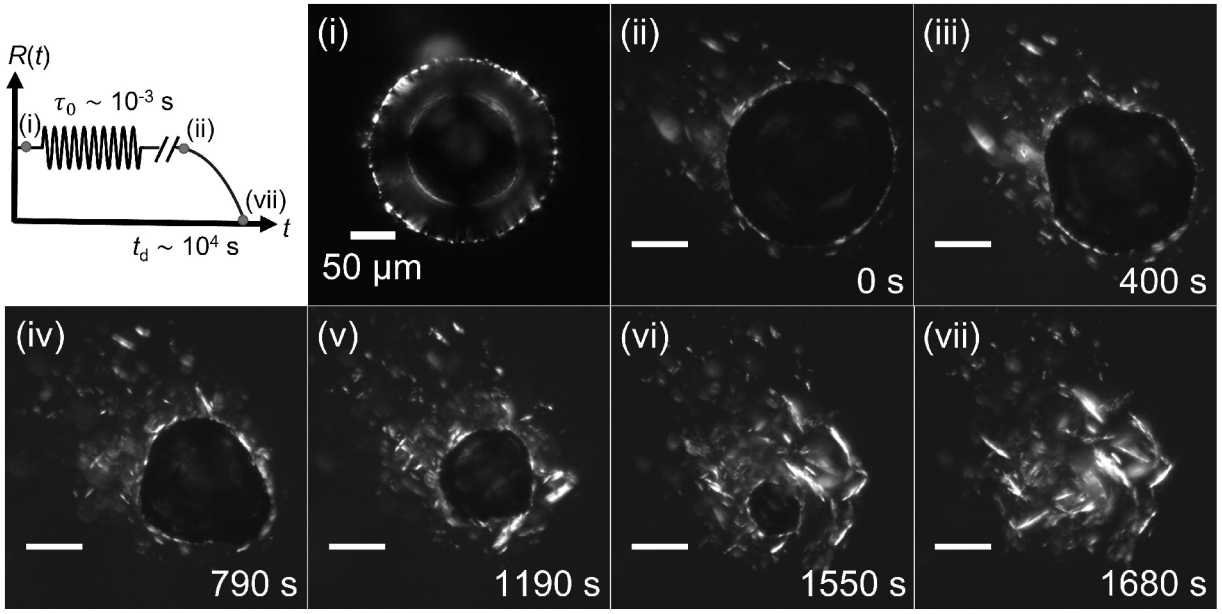

Figure 4. Bubble dissolution after ultrasound-driven bubble oscillations. The schematic shows the protocol including large-amplitude radial oscillations, followed by unperturbed dissolution. The labels correspond to the image sequence shown in panels i–vii. The initial radius of the bubble before oscillations (i) is R_0 = 102 μm. Oscillations are driven by ultrasound at f = 25 kHz for N = 480 cycles, with amplitude of oscillations x_0 > 20% (shown in SI Video 4). (ii) t = 0 s represents the start time of recording as the bubble dissolves (ii–vii).

observed. Typically, dissolution occurs over a time scale in the same range as for uncoated bubbles, $t_d \sim 10^3$–10^4 s.

Oscillation of Bubbles Using Ultrasound. To access short time scales of interface deformation, we exploit ultrasound-driven bubble oscillations. The periodic oscillations of the pressure around the ambient value, p_0, caused by an acoustic wave, force the gas core of a bubble to undergo periodic compression and expansion at the same frequency.[30] The driving frequency f was selected close to the natural frequency f_0 of a bubble of radius R_0 in an unbounded liquid. The relation between these quantities is given by the Minnaert frequency,[30] modified to include surface tension effects:

$$f_0 = \frac{1}{2\pi}\sqrt{\frac{3\kappa p_0 + 2\sigma/R_0}{\rho_l {R_0}^2}} \quad (2)$$

where κ is the polytropic exponent of the gas, taken to be 1.4 (assuming adiabatic behavior); σ is the surface tension; and ρ_l is the liquid density. For bubbles of radii $R_0 \approx 100$ μm, the driving frequencies were selected in the range $f_0 \sim 10$ kHz, leading to oscillatory deformation with a period

$$\tau_0 = \frac{1}{f_0} \approx 10^{-4}\ \text{s} \quad (3)$$

To transmit ultrasound waves into the sample and observe the dynamics of wax-coated bubbles, we used an ultrasound transducer (bolt-clamped Langevin transducer, Steminc; resonance frequency 25 kHz) glued onto a glass plate and driven by an arbitrary waveform generator (Agilent 33220A, Agilent Technologies, Inc.) connected to a linear power amplifier (AG 1021, T&C Power Conversion), as shown in Figure 1d. A sine wave of prescribed frequency f, acoustic pressure amplitude Δp, and number of cycles N was sent to the transducer by the waveform generator and amplifier. The ultrasound-driven bubble dynamics are recorded with a high-speed camera (FASTCAM SA5, Photron) connected to the inverted microscope. The frame rate used for the high-speed camera was at least 10 times the driving frequency. The amplitude of bubble oscillations, which is controlled both by the forcing frequency f and by the acoustic pressure amplitude Δp, is quantified from image analysis as $x_0 = \Delta R/R_0$, with ΔR the maximum amplitude of bubble oscillations and R_0 the equilibrium bubble radius.

RESULTS AND DISCUSSION

Experimental Observations. The dynamics of dissolution of a bubble in oil, stabilized by an interfacial layer of wax crystals, is shown in Figure 2 (Supporting Information (SI) Video 1). The schematic shows qualitatively the time evolution of the radius $R(t)$, and the different stages of the process are shown in images i–vii, which were taken with crossed polarizers to highlight the layer of crystals (seen as bright in the images). Between t = 4430 s and t = 5360 s (Figure 2iii,iv), a sharp deformation of the interface is observed on the right side of the bubble, from where a cohesive layer of crystals detaches as the bubble dissolves. Between t = 5960 s and t = 6400 s (Figure 2v,vi), there is again a sharp distortion to the left side of the bubble, followed by detachment of the layer from that location. Thus, detachment appears to initiate from the points of maximum deformation. At t = 7090 s, after the bubble has completely dissolved (Figure 2vii), a cohesive layer of crystals, seen as a bright spiral-like structure in the image, is left behind. The layer of crystals was observed to remain intact over months. The layer appears to be composed of large crystal rafts with characteristic dimension l comparable to the initial bubble radius ($R_0 \approx 100$ μm).

Figure 3 shows the effects of ultrasound-driven bubble oscillations of small and large amplitudes on the same wax-coated bubble. The frequency of oscillations is f = 25 kHz, and the bubble is successively excited by pulses of N cycles (two pulses of different amplitudes are shown in the schematic of Figure 3 by way of example). At moderate acoustic pressure, the amplitude of bubble oscillations is limited to $x_0 \approx 3\%$, too small to be clearly visible in Figure 3a, and more clearly visible in the corresponding SI Video 2, which shows a pulse of N = 50 cycles. The interface buckles during compression (Figure 3a-iii) and, over a total of N = 260 cycles, undergoes a clear change from the initial non-spherical shape (Figure 3a-i) to almost spherical shape (Figure 3a-iv). For the same bubble at higher acoustic pressures, the amplitude of oscillations

https://doi.org/10.1021/acs.langmuir.1c03171
Langmuir 2022, 38, 1259–1265

becomes $x_0 > 20\%$, which is clearly visible in the high-speed recording with crossed polarizers (SI Video 3) as well as in the corresponding image sequence in Figure 3b. The morphology of the crystal layer after large-amplitude oscillations at high frequency ($N = 100$ cycles) is profoundly different from the case of slow compression during bubble dissolution: crystals are expelled from the layer, which are much smaller than the initial bubble radius, $l \ll R_0$, seen in Figure 3b-viii. In contrast, the size of the segments forming the cohesive layer after bubble dissolution is $l \approx R_0$. Lastly, we examined the effect of ultrasound-driven oscillations on subsequent dissolution of wax-coated bubbles. Following a period of ultrasound-driven oscillations, the bubbles were left to dissolve completely, as shown in the schematic in Figure 4. Figure 4i shows a wax-coated bubble of initial radius $R_0 \approx 102$ μm before any deformation is applied. The bubble was first driven into large-amplitude oscillations ($x_0 > 20\%$) with ultrasound frequency $f = 25$ kHz, and for $N = 480$ cycles. After this number of cycles of oscillations, expulsion of a limited amount of crystals from the interface was obtained, without complete disruption of the interfacial layer, as seen in Figure 4ii. Forcing with ultrasound was stopped at this point, and the same bubble was then left to dissolve. An image sequence of the bubble dissolution steps is shown in Figure 4ii−vii (see also SI Video 3). The crystals and fragments of interfacial layer left behind after the bubble has completely dissolved ($t = 1680$ s; see Figure 4vii) appear larger compared to those that are expelled by ultrasound-driven oscillations; see Figure 3viii for comparison.

Mechanism of Layer Detachment for Slow Compression. Observations of the dissolution of wax-coated bubbles (sample size $n \approx 10$) indicate that, as the bubble decreases in size, the interfacial layer gradually detaches from the air−oil interface without significant changes in its morphology. In some instances ($n = 3$), the bubble remains fully covered with an interfacial layer during the entire process, until its complete dissolution (see Figure 2). These observations suggest that the energy penalty of deformation of the interfacial layer, measured by the compression modulus, exceeds the adhesive interaction energy between the wax layer and the air−oil interface. The compression modulus of the wax crystal layer on an air/oil interface was previously estimated[11] to be $K_d \approx 40-60$ mJ/m^2. As the interfacial layer detaches from the bubble interface, the inner surface of the (solid) wax crystal layer, initially in contact with air, becomes wetted by oil and a region of bare oil/air interface is formed. In this process, the change in interfacial energy per unit area can therefore be estimated to be in the range $\gamma_{os} + \gamma_{oa} - \gamma_{as} \approx 1-10$ mJ/m^2, with $\gamma_{oa} \approx 30$ mJ/m^2 the surface tension of the oil/air interface, $\gamma_{os} \approx 1-5$ mJ/m^2 the interfacial energy of the solid/oil interface, and $\gamma_{as} \approx 20-35$ mJ/m^2 the surface energy of the solid/air interface. It is therefore energetically favorable for the layer to detach from the gas interface during bubble dissolution, since the change in interfacial energy is small compared to the compression modulus. Comparing with the literature for clay-stabilized bubbles in alkanes[23] and latex-stabilized bubbles in water,[22] we identify two features common to all systems for when a continuous layer is left behind: the interface deformation is slow, occurring over a time scale $t_d \sim 10^3-10^4$ s, and the size of the particles is much smaller than the bubble radius, leading to a continuum behavior.[21]

Mechanisms of Crystal Expulsion for Fast Deformation. During ultrasound-driven bubble oscillations, the wax crystal layer undergoes rapid compression and expansion, as well as out-of-plane deformation due to buckling, shown in Figure 3a-iii, which can break the initially cohesive layer. This hypothesis is supported by the observation in Figure 3a that, for small-amplitude oscillations, the shape of the bubble changes without expulsion of interfacial material. The bubble becomes less non-spherical, consistent with an interfacial microstructure that cannot support anisotropic stresses. Because compression occurs on a very short time scale, $\tau_0 \sim 10^{-4}$ s, compared to rearrangement time scales in densely packed colloid monolayers, there is not sufficient time for rearrangement of the crystals to form a cohesive network. When a bubble that has been pre-treated with ultrasound-driven oscillations is allowed to dissolve (Figure 4), the interface undergoes slow compression, allowing sufficient time for the crystals to rearrange and form again a cohesive, solid-like network that can support anisotropic stresses as evidenced by the non-spherical shape of the bubble (Figure 4iii−v).

For bubble oscillations of large amplitude, several concurrent mechanisms can contribute to the expulsion of crystals, similar to observations for colloid-coated bubbles in water,[24] including significant out-of-plane buckling of the layer (SI Video 5). In the case of large-amplitude oscillations, when the same bubble is allowed to dissolve, the fragments of interfacial layer left behind are larger than those produced by ultrasound oscillations alone. This suggests that the large-amplitude oscillations can break the original interfacial structure but, following this, as the interface is compressed slowly there is sufficient time for the remaining crystals to rearrange and form larger cohesive rafts.

Finally, a secondary, slow flow called "microstreaming" and caused by bubble oscillations in confined geometries[31] cannot be ruled out in our experiments, but is not expected to disrupt the interfacial layer. We do not see direct evidence of microstreaming flow, but its effect would be to re-distribute expelled crystals along characteristic, closed streamlines around the bubble.

CONCLUSIONS

We investigated the response to deformation of an interfacial layer formed by a crystallizing agent on the surface of bubbles in an oil phase, at two extreme time scales that are, on one hand, relevant to the shelf life of such systems and, on the other hand, relevant to their processing and application. We found that the morphology of the interfacial layer is modified, depending on the interplay between the time scales of deformation and crystal rearrangement. For slow deformation, the crystals form a cohesive network, whereas for fast deformation the layer is fragmented. Conversely, the fate of the monolayer can be controlled by carefully combining these deformation protocols on the same layer. Also, depending on the requirement, the bubble shapes can be altered. These effects can find utility in modifying the morphology, rheology, and texture of foams in cosmetic and food applications. Furthermore, by tuning the timing and duration of ultrasound-induced deformation, protocols can be devised for the use of crystal-coated microbubbles for controlled release, useful for delivery of active pharmaceutical ingredients. Our findings pave the way for the design of stimuli-responsive systems that can be triggered to behave uniquely depending on the time scale of deformation, in addition to the already-known temperature dependence of the phase-changing stabilizing agent.

https://doi.org/10.1021/acs.langmuir.1c03171
Langmuir 2022, 38, 1259−1265

■ ASSOCIATED CONTENT

Supporting Information

The Supporting Information is available free of charge at https://pubs.acs.org/doi/10.1021/acs.langmuir.1c03171.

High-magnification optical micrographs and characterization of crystal shape and size in bulk oleogel network and at oil/air interface (PDF)

Dissolution of a wax-coated bubble in oil, imaged with crossed polarizers (MP4)

Small-amplitude oscillations (driven by ultrasound at 25 kHz) of a wax-coated bubble in oil (MP4)

Large-amplitude oscillations (driven by ultrasound at 25 kHz) of a wax-coated bubble in oil, imaged with crossed polarizers (AVI)

Dissolution of a wax-coated bubble after pre-treatment with large-amplitude ultrasound-driven oscillations, imaged with crossed polarizers (MP4)

Large-amplitude oscillations (driven by ultrasound at 25 kHz) of a wax-coated bubble showing buckling (AVI)

■ AUTHOR INFORMATION

Corresponding Author

Valeria Garbin − *Department of Chemical Engineering, Delft University of Technology, 2629 HZ Delft, The Netherlands; Department of Chemical Engineering, Imperial College London, London SW7 2AZ, United Kingdom;* orcid.org/0000-0002-0887-500X; Email: v.garbin@tudelft.nl

Authors

Saikat Saha − *Department of Chemical Engineering, Delft University of Technology, 2629 HZ Delft, The Netherlands; Department of Chemical Engineering, Imperial College London, London SW7 2AZ, United Kingdom*

Francis Pagaud − *Department of Chemical Engineering, Imperial College London, London SW7 2AZ, United Kingdom;* Present Address: Université de Lyon, École Normale Supérieure de Lyon, CNRS, Laboratoire de Physique, F-69342 Lyon, France

Bernard P. Binks − *Department of Chemistry, University of Hull, Hull HU6 7RX, United Kingdom;* orcid.org/0000-0003-3639-8041

Complete contact information is available at: https://pubs.acs.org/10.1021/acs.langmuir.1c03171

Notes

The authors declare no competing financial interest.

■ ACKNOWLEDGMENTS

The authors thank P. Luckham, J. Seddon, B. Dollet, and E. Wagner for helpful discussions. This work is supported by European Research Council Starting Grant No. 639221 (V.G.).

■ REFERENCES

(1) Fameau, A.-L.; Saint-Jalmes, A. Non-aqueous foams: Current understanding on the formation and stability mechanisms. *Adv. Colloid Interface Sci.* **2017**, *247*, 454−464.

(2) Heymans, R.; Tavernier, I.; Dewettinck, K.; Van der Meeren, P. Crystal stabilization of edible oil foams. *Trends Food Sci. Technol.* **2017**, *69*, 13−24.

(3) Fameau, A.-L.; Binks, B. P. Aqueous and oil foams stabilized by surfactant crystals: New concepts and perspectives. *Langmuir* **2021**, *37*, 4411−4418.

(4) Mishima, S.; Suzuki, A.; Sato, K.; Ueno, S. Formation and microstructures of whipped oils composed of vegetable oils and high-melting fat crystals. *J. Am. Oil Chem. Soc.* **2016**, *93*, 1453−1466.

(5) Gunes, D. Z.; Murith, M.; Godefroid, J.; Pelloux, C.; Deyber, H.; Schafer, O.; Breton, O. Oleofoams: Properties of crystal-coated bubbles from whipped oleogels−Evidence for Pickering stabilization. *Langmuir* **2017**, *33*, 1563−1575.

(6) Heymans, R.; Tavernier, I.; Danthine, S.; Rimaux, T.; Van der Meeren, P.; Dewettinck, K. Food-grade monoglyceride oil foams: the effect of tempering on foamability, foam stability and rheological properties. *Food Funct.* **2018**, *9*, 3143−3154.

(7) Liu, Y.; Binks, B. P. A novel strategy to fabricate stable oil foams with sucrose ester surfactant. *J. Colloid Interface Sci.* **2021**, *594*, 204−216.

(8) Binks, B. P.; Vishal, B. Particle-stabilized oil foams. *Adv. Colloid Interface Sci.* **2021**, *291*, 102404.

(9) Goibier, L.; Pillement, C.; Monteil, J.; Faure, C.; Leal-Calderon, F. Emulsification of non-aqueous foams stabilized by fat crystals: Towards novel air-in-oil-in-water food colloids. *Food Chem.* **2019**, *293*, 49−56.

(10) Saha, S. Micromechanics of Particle-Coated Bubbles: Deformation from Quasistatic to Millisecond Timescales. Ph.D. Thesis, Imperial College London, 2020.

(11) Saha, S.; Saint-Michel, B.; Leynes, V.; Binks, B. P.; Garbin, V. Stability of bubbles in wax-based oleofoams: decoupling the effects of bulk Oleogel rheology and interfacial rheology. *Rheol. Acta* **2020**, *59*, 255−266.

(12) Liascukiene, I.; Amselem, G.; Landoulsi, J.; Gunes, D. Z.; Baroud, C. N. Intermittent dynamics of bubble dissolution due to interfacial growth of fat crystals. *Soft Matter* **2021**, *17*, 10042−10052.

(13) Tavernier, I.; Moens, K.; Heyman, B.; Danthine, S.; Dewettinck, K. Relating crystallization behavior of monoacylglycerols-diacylglycerol mixtures to the strength of their crystalline network in oil. *Food Res. Int.* **2019**, *120*, 504−513.

(14) Metilli, L.; Lazidis, A.; Francis, M.; Marty-Terrade, S.; Ray, J.; Simone, E. The effect of crystallization conditions on the structural properties of oleofoams made of cocoa butter crystals and high oleic sunflower oil. *Cryst. Growth Des.* **2021**, *21*, 1562−1575.

(15) Fameau, A.-L.; Saint-Jalmes, A. Recent advances in understanding and use of oleofoams. *Frontiers Sust. Food Systems* **2020**, *4*, 110.

(16) Bala Subramaniam, A.; Abkarian, M.; Mahadevan, L.; Stone, H. A. Non-spherical bubbles. *Nature* **2005**, *438*, 930.

(17) Beltramo, P. J.; Gupta, M.; Alicke, A.; Liascukiene, I.; Gunes, D. Z.; Baroud, C. N.; Vermant, J. Arresting dissolution by interfacial rheology design. *Proc. Nat. Acad. Sci.* **2017**, *114*, 10373.

(18) Kam, S. I.; Rossen, W. R. Anomalous capillary pressure, stress, and stability of solids-coated bubbles. *J. Colloid Interface Sci.* **1999**, *213*, 329−339.

(19) Abkarian, M.; Subramaniam, A. B.; Kim, S.-H.; Larsen, R. J.; Yang, S.-M.; Stone, H. A. Dissolution arrest and stability of particle-covered bubbles. *Phys. Rev. Lett.* **2007**, *99*, 188301.

(20) Pitois, O.; Buisson, M.; Chateau, X. On the collapse pressure of armored bubbles and drops. *Eur. Phys. J. E* **2015**, *38*, 48.

(21) Taccoen, N.; Lequeux, F.; Gunes, D. Z.; Baroud, C. N. Probing the mechanical strength of an armored bubble and its implication to particle-stabilized foams. *Phys. Rev. X* **2016**, *6*, 011010.

(22) Poulichet, V.; Garbin, V. Cooling particle-coated bubbles: Destabilization beyond dissolution arrest. *Langmuir* **2015**, *31*, 12035−12042.

(23) Achakulwisut, K.; Tam, C.; Huerre, A.; Sammouti, R.; Binks, B. P.; Garbin, V. Stability of clay particle-coated microbubbles in alkanes against dissolution induced by heating. *Langmuir* **2017**, *33*, 3809−3817.

(24) Poulichet, V.; Garbin, V. Ultrafast desorption of colloidal particles from fluid interfaces. *Proc. Nat. Acad. Sci.* **2015**, *112*, 5932−5937.

(25) Kloek, W.; Van Vliet, T.; Meinders, M. Effect of bulk and interfacial rheological properties on bubble dissolution. *J. Colloid Interface Sci.* **2001**, *237*, 158−166.
(26) Mishra, K.; Grob, L.; Kohler, L.; Zimmermann, S.; Gstöhl, S.; Fischer, P.; Windhab, E. J. Entrance flow of unfoamed and foamed Herschel−Bulkley fluids. *J. Rheol.* **2021**, *65*, 1155−1168.
(27) Fameau, A.-L.; Lam, S.; Arnould, A.; Gaillard, C.; Velev, O. D.; Saint-Jalmes, A. Smart nonaqueous foams from lipid-based oleogel. *Langmuir* **2015**, *31*, 13501−13510.
(28) Duncan, P. B.; Needham, D. Test of the Epstein-Plesset model for gas microparticle dissolution in aqueous media: Effect of surface tension and gas undersaturation in solution. *Langmuir* **2004**, *20*, 2567−2578.
(29) Epstein, P. S.; Plesset, M. S. On the stability of gas bubbles in liquid-gas solutions. *J. Chem. Phys.* **1950**, *18*, 1505−1509.
(30) Plesset, M. S.; Prosperetti, A. Bubble dynamics and cavitation. *Annu. Rev. Fluid Mech.* **1977**, *9*, 145−185.
(31) Bolaños-Jiménez, R.; Rossi, M.; Fernandez Rivas, D.; Kähler, C. J.; Marin, A. Streaming flow by oscillating bubbles: quantitative diagnostics via particle tracking velocimetry. *J. Fluid Mech.* **2017**, *820*, 529−548.

https://doi.org/10.1021/acs.langmuir.1c03171
Langmuir 2022, 38, 1259−1265